Journal of Materials Chemistry C

ROYAL SOCIETY OF CHEMISTRY

PAPER

View Article Online
View Journal

Cite this: DOI: 10.1039/d0tc03285a

White-light electroluminescence from a layer incorporating a single fully-organic spiro compound with phosphine oxide substituents†

P. Tourneur,‡[a] F. Lucas,‡[b] C. Quinton,[b] Y. Olivier,[c] R. Lazzaroni,[ad] P. Viville,[d] J. Cornil *[a] and C. Poriel *[b]

Received 12th July 2020,
Accepted 30th September 2020

DOI: 10.1039/d0tc03285a

rsc.li/materials-c

We have investigated the potential as an OLED emitter of a spiro compound with phosphine substituents initially designed as a host layer for triplet emitters. This is motivated by the fact that the spiro architecture is expected to reduce the detrimental impact of intermolecular interactions, thus allowing for the use of a single-component layer. Moreover, theoretical calculations suggest that this compound displays all features required for a thermally-assisted delayed fluorescence (TADF) behavior. The photophysical properties of the compound in solution are extremely unusual, as illustrated in particular by a dual emission band with relative intensities strongly depending on the experimental conditions. Although no TADF behavior is evidenced in OLED devices, the compound unexpectedly generates a white light signal, which is interpreted as the result of the formation of both intramolecular and intermolecular (exciplex) charge-transfer states.

Introduction

Despite the tremendous commercial success of the organic light-emitting diode (OLED) technology, the field is still searching for strategies to build devices incorporating fully-organic emitters together with a small number of layers in order to reduce the production costs.[1,2]

On the one hand, the first challenge stems from the need to replace the widely used organometallic complexes due to the toxicity and/or low earth abundance of the metallic centres, such as iridium, platinum, or osmium.[3] Nevertheless, the substitutes should preserve the huge benefit accompanying the use of organometallic dopants, namely the full harvesting of the electron–hole pairs into triplet excitons exploitable for phosphorescence emission thanks to the large spin–orbit coupling provided by the metallic centers,[4] leading to external quantum yields frequently reported above 25% for red, green, and blue emission.[5–10] This has stimulated recently a large amount of work dedicated to Thermally Assisted Delayed Fluorescence (TADF).[3,11–13] Here, the key idea is to design fully-organic molecules featuring a small energy gap ΔE_{ST} (typically below 200 meV) between the lowest singlet and triplet excited state in order to convert by thermal activation the triplet excitons into singlet excitons *via* a reverse intersystem crossing process (RISC);[14–16] the singlet excitons can then decay radiatively with a short lifetime component linked to the intrinsic fluorescence decay (*i.e.* the prompt fluorescence) and a long-lived component originating from the triplet exciton reconversion (*i.e.* the delayed fluorescence). A small ΔE_{ST} is typically achieved by designing molecules with a pronounced charge-transfer character in the lowest excited state, *i.e.*, with a distinct spatial localization of the HOMO and LUMO wavefunctions[3] in order to reduce the exchange energy term.

On the other hand, standard TADF and phosphorescent OLED devices include host–guest systems to reduce the detrimental impact of intermolecular interactions on the solid-state luminescence properties[17–19] thus requiring a critical choice of the components to ensure a proper energy level alignment of the electronic levels (HOMO/LUMO) and excited states (S_1 and T_1) to transfer the excitons efficiently to guest species. Moreover, the experimental processing conditions should be finely tuned so that the host–guest systems feature a good dispersion of the emitting dopants within the matrix. One strategy reported in the early days of the field to alleviate this drawback is to exploit spiro compounds to limit the impact of intermolecular interactions thanks to their cumbersome 3D shapes.[20] This strategy has also been successfully employed, with the flagship 9,9′-spirobifluorene molecule, for the design of

[a] Laboratory for Chemistry of Novel Materials, Materials Research Institute, University of Mons, Mons, Belgium. E-mail: jerome.cornil@umons.ac.be
[b] Université de Rennes, CNRS, ISCR-UMR 6226, F-35000 Rennes, France. E-mail: cyril.poriel@univ-rennes1.fr
[c] Unité de Chimie Physique Théorique et Structurale (UCPTS) & Laboratoire de Physique du Solide (LPS), Namur Institute of Structured Matter (NISM), University of Namur, Namur, Belgium. E-mail: yoann.olivier@unamur.be
[d] Materia Nova, Materials R&D center, Mons, Belgium. E-mail: pascal.viville@materianova.be

† Electronic supplementary information (ESI) available. See DOI: 10.1039/d0tc03285a

‡ First authorship shared.

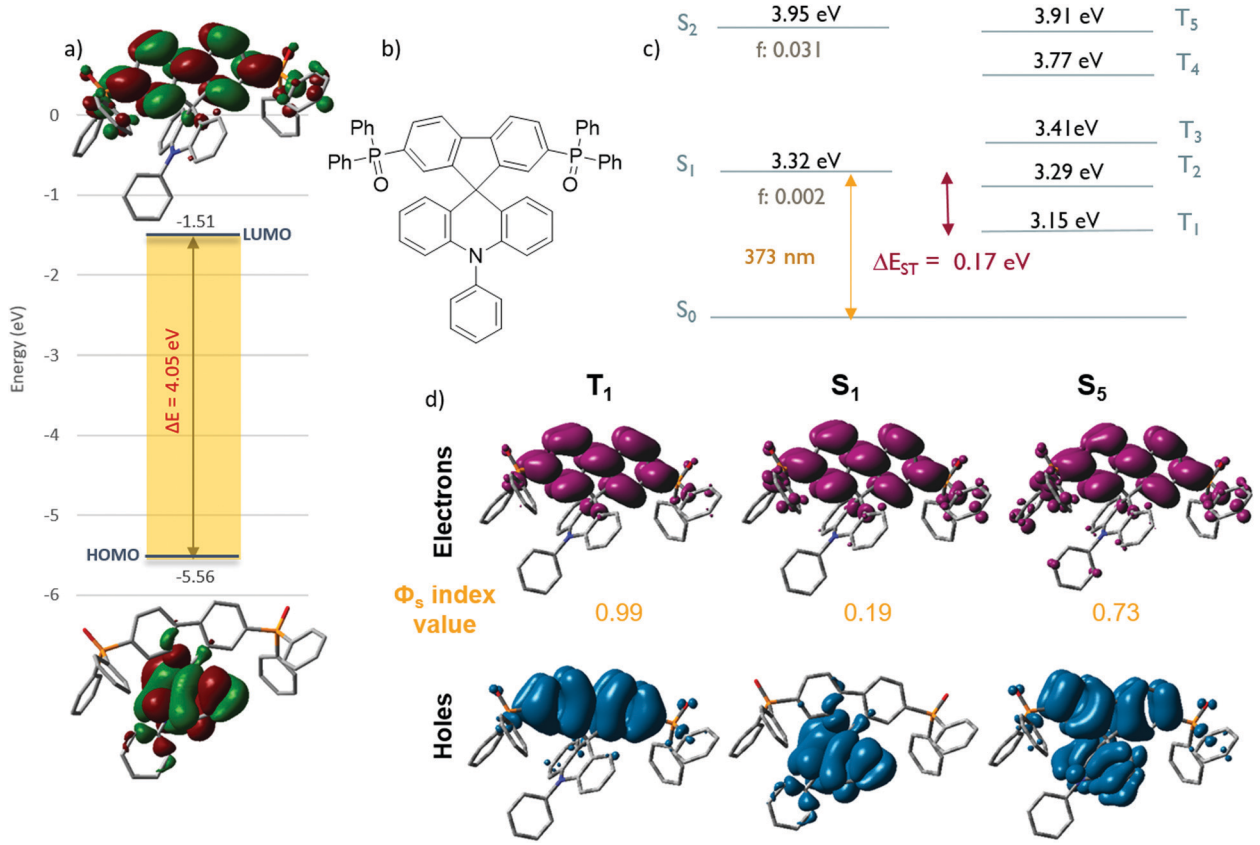

Fig. 1 (a) Shape of the HOMO (bottom) and LUMO (top) levels of **SPA-F(POPh$_2$)$_2$** in its ground state geometry, (b) chemical structure of the compound, (c) energies of the lowest singlet and triplet excited states and oscillator strengths associated to the singlet states, (d) plots of the electron detachment/attachment densities of S_1, T_1, and S_5. These results have been obtained at the (TD-)DFT level with the PBE0 functional and the represented surfaces have been obtained using an isocontour value of 0.02.

high-triplet-energy host materials for phosphorescent OLEDs.[21,22] Recently, this molecular approach has been adopted with some spiro-based TADF compounds used in a single emissive layer[23] in contrast to many previous works involving spiro-based TADF emitters in a host matrix.[24–26]

The above considerations have motivated us to explore the potential of single-component layers based on a donor–acceptor spiro compound for light emission in OLED devices. Actually, some of us have recently synthesized a compound matching all requirements, namely the spirophenylacridine-2,7-(diphenylphosphineoxide)-fluorene compound (**SPA-F(POPh$_2$)$_2$**, Fig. 1), which connects *via* a central spiro carbon an electron-rich phenylacridine unit (acting as electron donor) and an electron-deficient 2,7-bis-(diphenylphosphine oxide)-fluorene, acting as electron acceptor. Note that this compound was initially designed for a completely different purpose, namely as host matrix for green and blue single-layer phosphorescent OLEDs.[27] In this work, we report a detailed characterization of the unusual absorption and emission properties of this compound both in solution and thin films. The experimental results have been further rationalized with the help of theoretical modelling. Strikingly, when inserted in OLED devices as a single emissive layer, this compound yields a white light emission that we interpret as originating from the contributions of a mixture of emitting intramolecular and intermolecular charge-transfer excited states. This clearly represents a huge benefit in terms of stability and processing compared to white emitting OLED devices typically incorporating several emitters.[28]

Results and discussion

We have first explored the electronic and optical properties of this compound by computing its electronic levels and excited states at the (Time-Dependent) Density Functional Theory – (TD)-DFT – level. These calculations have been performed using the hybrid PBE0 functional and a 6-31G** basis set; the TD-DFT calculations have been performed within the Tamm–Dancoff approximation; its validity has been assessed in previous studies.[29–31] As expected, the HOMO of the molecule is strongly localized on the acridine group and the LUMO localized on the fluorene group (Fig. 1). The lowest singlet excited state S_1 is calculated at 3.32 eV in the gas phase and is only weakly optically coupled to the ground state (oscillator strength = 0.002); this also holds true for the singlet states from S_2 to S_4, with oscillator strengths of 0.031, 0.004, and 0.001, respectively. The first singlet state strongly coupled to the ground state is the fifth excited state (S_5) lying 0.92 eV above S_1. The lowest triplet state is computed at 3.15 eV, thus leading to a small ΔE_{ST} of

0.17 eV. We have also used the detachment/attachment formalism to visualize the electronic density removed in the ground state upon excitation (detachment) and the way it is rearranged in the excited state (attachment).[32] In this framework, the overlap Φ_S between the electron and hole density is a useful parameter to gauge the degree of charge-transfer (CT) character in an excited state;[31,33,34] $\Phi_S = 1$ for a purely localized character (over either the donor or the acceptor part) and 0 for a pure CT excitation. In the case of this spiro compound, $\Phi_S = 0.99$ in T_1 and 0.19 in S_1 (Fig. 1), clearly pointing to the difference in the nature of those two states, which favors efficient reverse intersystem crossing in the TADF mechanism according to El Sayed rules.[35] At the same level theory, the prototypical **2CzPN** TADF emitter (see chemical structure in Fig. 9) exhibits a larger S_1–T_1 splitting (0.34 eV) than **SPA-F(POPh$_2$)$_2$**. The S_1 state of **2CzPN** lies about 0.3 eV below the value computed for the spiro compound; a major difference is, however, the large oscillator strength associated to the S_1 state in **2CzPN** (0.08 *versus* 0.002 in **SPA-F(POPh$_2$)$_2$**). This is readily explained by the fact that the donor and acceptor branches are orthogonal in the spiro compound, thus strongly limiting the electronic coupling between the HOMO and LUMO orbitals mostly involved in the $S_0 \rightarrow S_1$ excitation; this coupling is more pronounced in **2CzPN** featuring torsion angles around 60° between the donor and acceptor units. The Φ_S value of the S_1 state of **2CzPN** amounts to 0.42, thus pointing to a weaker charge-transfer character compared to **SPA-F(POPh$_2$)$_2$** ($\Phi_S = 0.19$).

Fig. 2 displays the absorption spectrum of **SPA-F(POPh$_2$)$_2$** recorded in THF together with the corresponding TD-DFT simulated spectrum; note that the spectrum simulated in gas phase has been shifted rigidly by 0.42 eV to higher energy to best match the most intense experimental absorption bands. The comparison between the experimental and theoretical spectra indicates that the first intense absorption band at 324 nm (3.82 eV) corresponds to S_5 and that the S_1 state is not observed in the spectra due to its very low oscillator strength (as can be understood from its pronounced charge-transfer character and the orthogonality of the donor and acceptor units imposed by the spiro centre). S_5 is an excited state mostly centred over the acceptor part with an $\Phi_S = 0.73$ (Fig. 1). The intramolecular character of S_5 is consistent with its large oscillator strength and Φ_S index, as well as the absence of significant solvatochromic effects (see Fig. S1, ESI†).

The emission properties of **SPA-F(POPh$_2$)$_2$** are extremely unusual. The emission spectrum recorded at room temperature in THF at a concentration of 4.4×10^{-5} mol L^{-1} displays a broad band centred around 490 nm. When the solution is warmed above 40 °C before recording spectra back at room temperature, the absorption spectrum remains unchanged while the emission spectrum exhibits an additional weak and broad band at higher energy, at *ca.* 400 nm (Fig. 3 and Fig. S2, ESI†). This new band keeps increasing with the heating time (Fig. 3), possibly suggesting that reaching another molecular conformation higher in energy might be required to observe that emission signal. The band systematically persists upon cooling down the solution to room temperature. At higher concentration (above 6.0×10^{-5} mol L^{-1}), the band at 400 nm is not observed, even at reflux of THF. Although this high-energy band does not play any role in the electroluminescence properties (*vide infra*), we performed some additional measurements to shed further light on its origin. We also emphasize that **2CzPN** does not display such a dual emission both in THF solution and film, see Fig. S3 (ESI†). This is most probably due to the larger electronic coupling between the donor and acceptor moieties ensuring that the system rapidly relaxes down to the S_1 state before emission occurs.

At a concentration of 4.8×10^{-5} mol L^{-1}, the excitation spectrum generated from the emission at 520 nm matches fairly well the shape of the absorption spectrum (Fig. 4, right). The high intensity of the excitation spectrum below 320 nm indicates that most electron–hole pairs photogenerated above

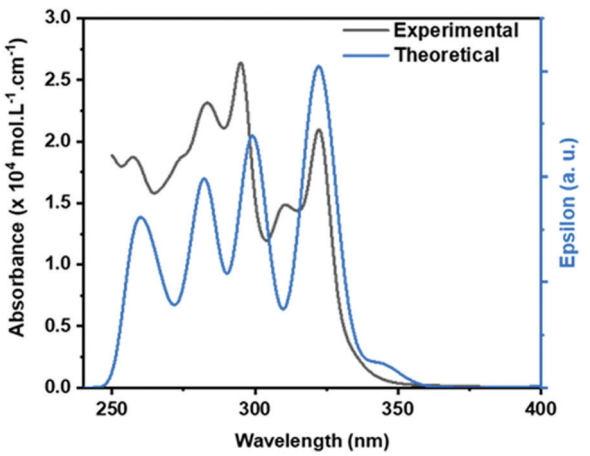

Fig. 2 Experimental absorption spectrum of **SPA-F(POPh$_2$)$_2$** in THF and corresponding TD-DFT simulated spectrum (full width at half maximum set to 0.1 eV).

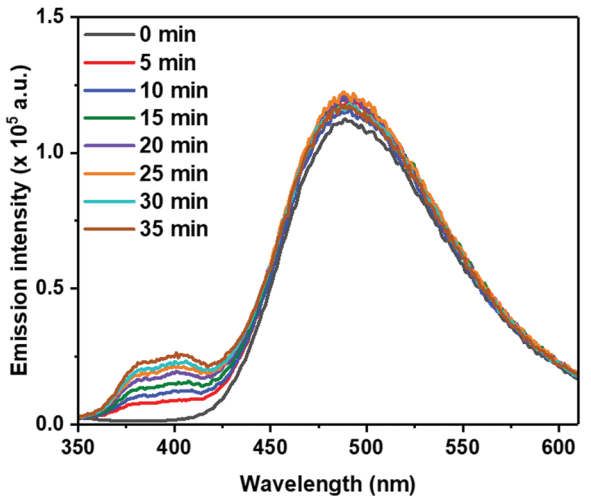

Fig. 3 Evolution as a function of heating time of the emission spectrum of **SPA-F-(POPh$_2$)$_2$** in THF at a concentration of 4.4×10^{-5} mol L^{-1} (with an excitation wavelength at 310 nm). The solution is heated at a constant temperature of 50 °C; 10 mL are extracted every 5 minutes and the emission spectra are recorded once the extracted solution has cooled down to room temperature.

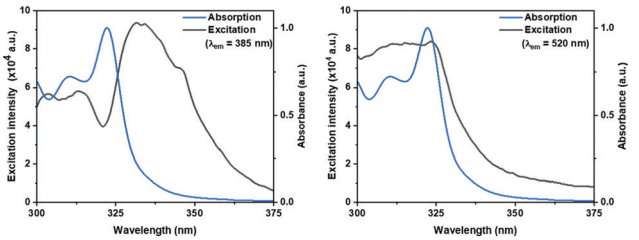

Fig. 4 Excitation (black lines) and absorption (blue lines) spectra of **SPA-F(POPh$_2$)$_2$** in THF. Excitation spectra have been recorded at λ_{em} = 385 nm (left) and λ_{em} = 520 nm (right) at a concentration of 4.8 × 10^{-5} mol L^{-1}; note that we have not measured the excitation spectra at energies corresponding to the maxima of the two emission bands in order to avoid any bias due to their overlap.

this energy threshold decay non-radiatively down to S_1 before emission occurs from that state. Strikingly, the excitation spectrum recorded at 385 nm (Fig. 4, left) overlaps poorly with the absorption spectrum and displays actually a high intensity in an energy range below the onset of the first intense absorption band, thus suggesting that the emission occurs from one (or several) excited state(s) lying higher than S_1. This is further supported by the variations in the emission spectra measured at different excitation wavelengths (Fig. 5): exciting above the energy of the first intense absorption band (<330 nm) favours the emission around 500 nm while excitation at higher wavelength (>330 nm) triggers the emission at 385 nm. Note that chemical degradation can be ruled out as an explanation for the appearance of the emission band at 385 nm because the absorption spectrum is not affected by heating.

The emission at low energy exhibits a significant solvatochromic effect (Fig. S4, ESI†), thus pointing to a strong charge-transfer character, as fully supported by the calculations (Fig. 1). Adding water progressively (from 0 to 38%) to the THF solution previously warmed above 40 °C leads to an increase and a red shift of the low energy emission band (Fig. S5, ESI†), which we

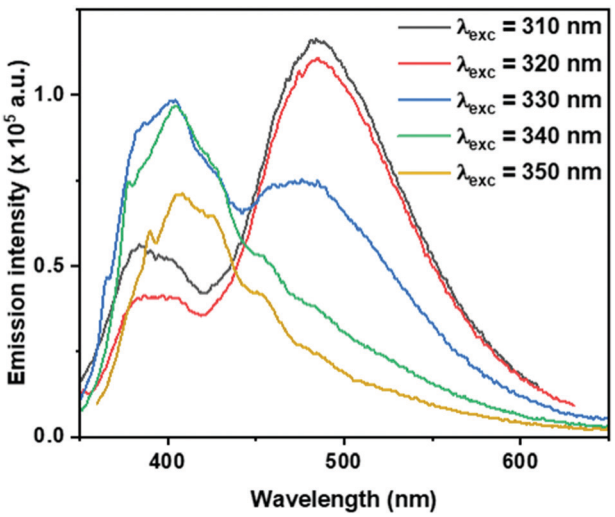

Fig. 5 Emission spectra of **SPA-F(POPh$_2$)$_2$** in THF at a concentration of 4.8 × 10^{-5} mol L^{-1}, as a function of the excitation wavelength.

associate to an interplay between the formation of aggregates induced by hydrophobic effects and the increase in the medium polarity. In contrast, the band at 385 nm is reduced in intensity but is not shifted, thus pointing to a locally excited character for this band.

The fluorescence decay curve of **SPA-F(POPh$_2$)$_2$** measured in THF at λ_{em} = 485 nm (λ_{exc} = 310 nm, see Fig. S6, ESI†) is dominated by a long lifetime of 11.5 ns; at λ_{em} = 354 nm, the fluorescence decays with a very short lifetime of 2.4 ns. This is once again coherent with the fact that S_1 has a strong charge-transfer character, in contrast to the state(s) at the origin of the emission at 385 nm. Interestingly, the same two emission bands are also observed when recording the spectra under argon (Fig. S7, ESI†); noteworthy, the intensity of the band at 500 nm is significantly increased in the absence of oxygen, thus pointing to the active role of triplet excitons in that band.[36] The quantum yield, using quinine sulfate as reference, is increased from below 1% under air to 4% under argon (see Fig. S7, ESI†). For the sake of comparison, the quantum yield of **2CzPN** has been reported at 28% in toluene.[37] This major difference is attributed to the large oscillator strength between S_0–S_1 in **2CzPN**, which makes fluorescence competitive with non-radiative decay channels, in contrast to the situation prevailing for **SPA-F(POPh$_2$)$_2$**.

However, the absence of a long tail extending up to the microsecond timescale in the decay emission profile of the band at 500 nm suggests the absence of a delayed fluorescence mechanism both in air and under argon in the present experimental conditions (see Fig. S5, ESI†). Altogether, we can conclude that the emission at 385 nm competes with the emission from S_1 at 480 nm following a branching ratio extremely sensitive to the excitation wavelength, temperature, time (possibly *via* conformational effects), and aggregation/concentration effects (possibly *via* electrostatic effects associated to the polar phosphine groups).

We have next deposited **SPA-F(POPh$_2$)$_2$** on glass both by spin coating at room temperature and by thermal sublimation. Fig. 6 compares the emission spectrum of the compound in solution (concentration below 6.0 × 10^{-5} mol L^{-1}) *versus* the solid state. In these experimental conditions, the two emission bands are observed in solution and in the vacuum-deposited thin films. In contrast, only the low energy band is observed for the spin-coated films, with a slight red shift of 19 nm (0.1 eV) compared to the solution, thus suggesting that the film morphology varies as a function of the processing method. We also typically observe an increased broadening of the main emission band on the low energy side in the solid state. This behaviour can be rationalized by the fact that an intermolecular charge-transfer state between the donor branch of one molecule and the acceptor branch of another (also referred to as exciplex) can significantly contribute to the spectra in the solid state, in addition to the intramolecular charge-transfer state characteristic of the isolated molecules in solution.[38] The large diversity of possible exciplex contact geometries is consistent with the larger spectral width observed in the thin film.

Finally, we have introduced a single layer of **SPA-F(POPh$_2$)$_2$** in bottom-emitting OLED devices. Since the present work does

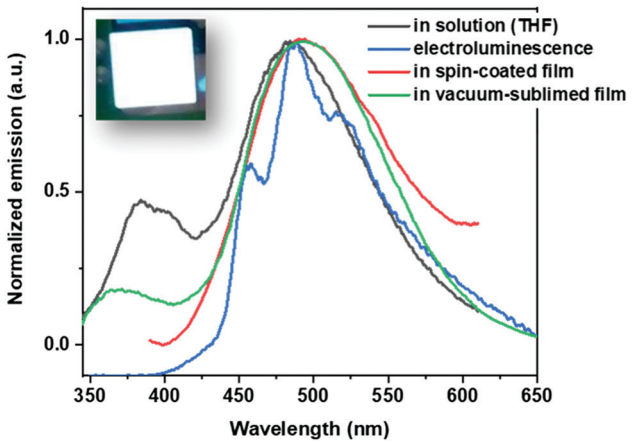

Fig. 6 Photoluminescence spectra of **SPA-F(POPh$_2$)$_2$** in THF (at a concentration of 4.75 × 10^{-5} mol L^{-1}) and in films deposited by spin-coating or thermal sublimation together with the electroluminescence signal recorded at 7 volts. The photoluminescence spectra have been recorded upon excitation at 310 nm.

not aim at optimizing the efficiency of the OLEDs, the devices were fabricated by thermal sublimation in a glovebox in a way inspired by the architecture typically used for the benchmark **2CzPN** TADF emitter (see chemical structure in Fig. 9):[11] a layer of 25 nm of a hole-injecting *N*,*N*-bis(naphthalen-1-yl)-*N*,*N*′-bis-(phenyl)-2,2′-dimethylbenzidine (**α-NPD**) compound was deposited on a commercial ITO (indium tin oxide)-covered glass substrate used as the anode, followed by 5 nm of a hole-transporting 1,3-bis(*N*-carbazolyl)benzene (**mCP**) layer, a 20 nm-thick layer of the **SPA-F(POPh$_2$)$_2$** emitter, 5 nm of bis[2-(diphenylphosphino)phenyl] ether oxide (**DPEPO**) as electron transport and hole-blocking material, 25 nm of 2,2′,2″-(1,3,5-benzinetriyl)-tris(1-phenyl-1-*H*-benzimidazole) (**TPBi**) as electron transport layer. Finally, a very thin layer (1 nm) of lithium fluoride facilitating electron injection and a 100 nm-thick Al layer as the cathode were deposited to complete the stack (Fig. 7). A detailed protocol for the fabrication of the devices is provided in the ESI.† Ultimately, 30 nm of Al_2O_3 were deposited by Atomic Layer Deposition (ALD) on top of the stack in order to encapsulate the devices prior to measurements of the performances outside the glovebox. We display in Fig. 7 the chemical structures of those compounds, as well as the relative alignment of their frontier electronic levels based on typical values reported in the literature.[39]

Strikingly, white light is generated by the OLEDs containing **SPA-F(POPh$_2$)$_2$**, with CIE chromatic coordinates of (0.26; 0.40). The spectral range of the electroluminescence signal is broad (from 400 nm to 750 nm, see blue curve in Fig. 6) and is very similar to that of the low energy photoluminescence signal obtained for thermally sublimed thin films. The electroluminescence spectrum also displays a more pronounced tail on the low energy side, suggesting that the concomitant emission from intramolecular and intermolecular excited states is at the origin of the white light. The electroluminescence signal is vibronically-resolved, in contrast to the photoluminescence spectra (both in solution and in films); this is most probably due to the fact that the injected carriers are thermalized in the emitting layer before they recombine radiatively from the low-energy CT states. Interestingly, the emission at 375 nm is not observed in the electroluminescence signal, as also expected from the fact that the thermalized injected electrons and holes do not recombine into the emitting high-lying excited state(s). Fig. 8 shows the evolution of the electroluminescence spectra as a function of the applied bias and points to the stability of the device at high voltage. At 8 volts, the current density reaches a value close to 200 mA cm^{-2} (see Fig. 9) while maintaining the shape of electroluminescent signal quite stable.

Finally, we have compared the electrical characteristics of OLEDs made from **SPA-F(POPh$_2$)$_2$** with those obtained for the prototypical **2CzPN** TADF blue emitter in a **mCP** matrix (see chemical structure in Fig. 9). The comparison is here performed with home-made devices fabricated with an architecture similar to that described in ref. 6 (namely **α-NPD** (30 nm)/**mCP:2CzPN** (25 nm–10 wt%)/TPBi (70 nm)/LiF (1 nm)/Al (100 nm)). We stress

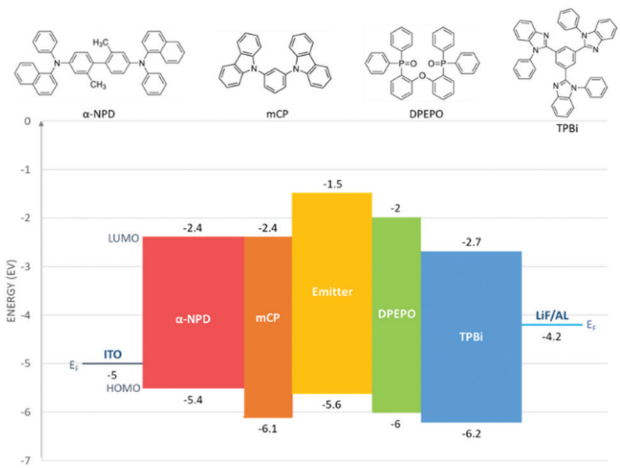

Fig. 7 Chemical structure of the compounds used in the different layers (**α-NPD**, **mCP**, **DPEPO** and **TPBi**, respectively) and scheme of the level alignment in the devices, based on typical values reported in the literature.[37]

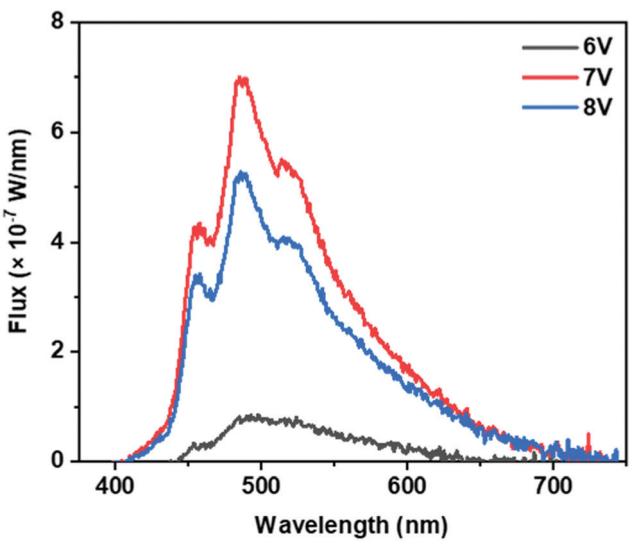

Fig. 8 Electroluminescence spectra recorded at different voltages.

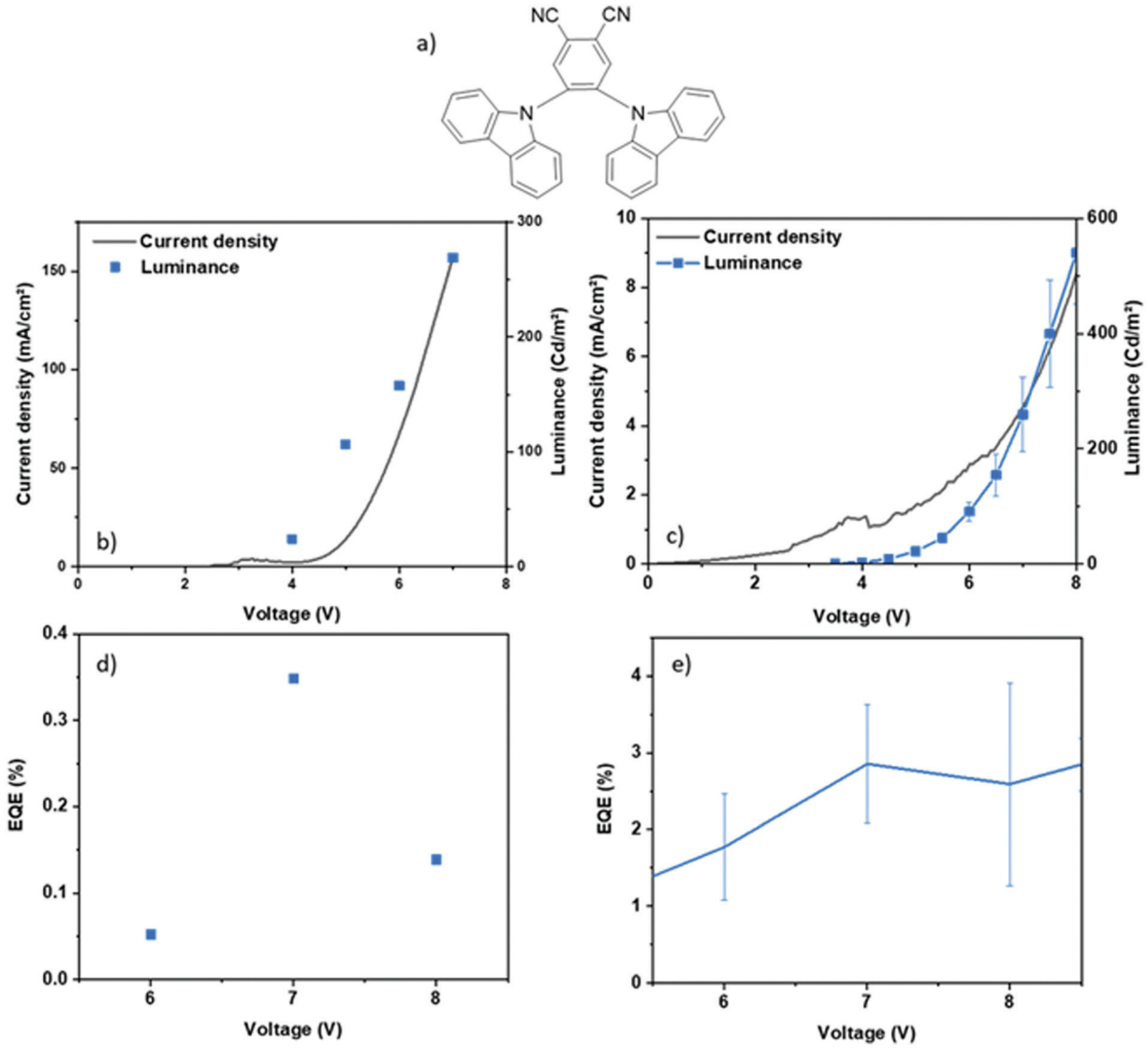

Fig. 9 Structure of **2CzPN** (a); luminance and current density curves of **SPA-F-(POPh$_2$)$_2$** and **2CzPN** (b and c, respectively); external quantum efficiency calculated from the electroluminescence spectra for **SPA-F-(POPh$_2$)$_2$** and **2CzPN** (d and e, respectively).

that the device fabrication with **2CzPN** was carried out in order to guarantee that the two series of devices under comparison have the same area (0.21 cm^2) and operate in the same experimental conditions, without optimization steps.

The devices based on **SPA-F(POPh$_2$)$_2$** show a low turn-on voltage (V_{ON}) of 4.5 V, very similar to that obtained when using **2CzPN/mCP** as emitting layer, with a higher current density (around 160 mA cm^{-2} in comparison with only 6.5 mA cm^{-2} for **2CzPN** at 7 V). The fact that a much higher current is observed can be linked to the architecture of the **SPA-F(POPh$_2$)$_2$** devices, which only comprise homogeneous layers rather than host–guest structures as in standard devices. The luminance measured at 7 V reaches 270 cd m^{-2} for **SPA-F(POPh$_2$)$_2$** and is slightly higher than with **2CzPN** (260 Cd m^{-2} at 7 V). The EQE reaches a value at 0.35% at 7 V, which is lower than the EQE obtained with **2CzPN** at the same bias (2.9%); note also that the EQE value obtained for **2CzPN** is fully consistent with that reported by Adachi and coworkers.[11] These results illustrate a disadvantage of the single-component layer, namely the fact the absence of a guest species strongly reduces the possibility of the charge trapping, and hence their more efficient recombination. There is a clear interest of using a single-component emissive layer for the fabrication of white light-emitting device, although a compromise appears necessary at this stage between the device efficiency and the easiness of device fabrication.

Conclusions

In this work, we unravelled the spectroscopic properties of an organic semi-conductor **SPA-F(POPh$_2$)$_2$** built on the association of an electron-rich (phenylacridine) and an electron-poor (diphenylphosphine oxide fluorene) fragment. In particular, we evidenced a very unusual dual emission, with the relative intensities of the two bands strongly affected by many factors such as the concentration and the

temperature in solution or the processing method in thin films. Theoretical calculations were further exploited to shed light on the nature of the lowest singlet excited states and to rationalize the spectroscopic measurements. When used as emitter in a single-component layer within an OLED, **SPA-F(POPh$_2$)$_2$** yields surprisingly a white light emission. This behaviour is attributed to the simultaneous occurrence of emission from intramolecular and intermolecular charge-transfer excited states, giving rise to a large distribution of electron–hole separations and hence of charge-transfer state energies at the origin of the spectral broadening in the film. With respect to white-emitting OLEDs typically incorporating several emitters,[28] the present work offers an alternative strategy, which needs to be optimized to ultimately fabricate devices with attractive quantum yield combined with simplified processing.

Conflicts of interest

There are no conflicts to declare.

Acknowledgements

This study benefited from the European Union through the Interreg V initiative France-Wallonie-Vlaanderen – projet LUMINOPTEX – and has been supported in Mons by the Belgian National Fund for Scientific Research (FRS-FNRS). Computational resources were provided by the Consortium des Équipements de Calcul Intensif (CÉCI) funded by F. R. S.-FNRS under Grant 2.5020.11. J. C. is an FNRS research director. The authors would like to thank the ANR (no. 19-CE05-0024) and the Region Bretagne (DIADEM project) for PhD grant (Fabien Lucas).

Notes and references

1 N. B. Kotadiya, P. W. M. Blom and G.-J. A. H. Wetzelaer, *Nat. Photonics*, 2019, **13**, 765–769.
2 C. Poriel and J. Rault-Berthelot, *Adv. Funct. Mater.*, 2020, **30**, 1910040.
3 Y. Liu, C. Li, Z. Ren, S. Yan and M. R. Bryce, *Nat. Rev. Mater.*, 2018, **3**, 18020.
4 M. A. Baldo, D. F. O'Brien, Y. You, A. Shoustikov, S. Sibley, M. E. Thompson and S. R. Forrest, *Nature*, 1998, **395**, 151–154.
5 Q. Wang, F. Lucas, C. Quinton, Y.-K. Qu, J. Rault-Berthelot, O. Jeannin, S.-Y. Yang, F.-C. Kong, S. Kumar, L.-S. Liao, C. Poriel and Z.-Q. Jiang, *Chem. Sci.*, 2020, **11**, 4887–4894.
6 K.-H. Kim, S. Lee, C.-K. Moon, S.-Y. Kim, Y.-S. Park, J.-H. Lee, J. Woo Lee, J. Huh, Y. You and J.-J. Kim, *Nat. Commun.*, 2014, **5**, 4769.
7 X.-Y. Liu, X. Tang, Y. Zhao, D. Zhao, J. Fan and L.-S. Liao, *ACS Appl. Mater. Interfaces*, 2018, **10**, 1925–1932.
8 C. W. Lee and J. Y. Lee, *Adv. Mater.*, 2013, **25**, 5450–5454.
9 A. Maheshwaran, V. G. Sree, H.-Y. Park, H. Kim, S. H. Han, J. Y. Lee and S.-H. Jin, *Adv. Funct. Mater.*, 2018, **28**, 1802945.
10 L. Ding, S.-C. Dong, Z.-Q. Jiang, H. Chen and L.-S. Liao, *Adv. Funct. Mater.*, 2015, **25**, 645–650.
11 H. Uoyama, K. Goushi, K. Shizu, H. Nomura and C. Adachi, *Nature*, 2012, **492**, 234–238.
12 M. Y. Wong and E. Zysman-Colman, *Adv. Mater.*, 2017, **29**, 1605444.
13 P. L. dos Santos, M. K. Etherington and A. P. Monkman, *J. Mater. Chem. C*, 2018, **6**, 4842–4853.
14 Y. Olivier, B. Yurash, L. Muccioli, G. D'Avino, O. Mikhnenko, J. C. Sancho-García, C. Adachi, T.-Q. Nguyen and D. Beljonne, *Phys. Rev. Mater.*, 2017, **1**, 075602.
15 X.-K. Chen, D. Kim and J.-L. Brédas, *Acc. Chem. Res.*, 2018, **51**, 2215–2224.
16 M. K. Etherington, J. Gibson, H. F. Higginbotham, T. J. Penfold and A. P. Monkman, *Nat. Commun.*, 2016, **7**, 13680.
17 J. Cornil, D. A. dos Santos, X. Crispin, R. Silbey and J. L. Brédas, *J. Am. Chem. Soc.*, 1998, **120**, 1289–1299.
18 Y. Tao, C. Yang and J. Qin, *Chem. Soc. Rev.*, 2011, **40**, 2943.
19 T. Chatterjee and K.-T. Wong, *Adv. Opt. Mater.*, 2019, **7**, 1800565.
20 T. P. I. Saragi, T. Spehr, A. Siebert, T. Fuhrmann-Lieker and J. Salbeck, *Chem. Rev.*, 2007, **107**, 1011–1065.
21 C. Poriel, L. Sicard and J. Rault-Berthelot, *Chem. Commun.*, 2019, **55**, 14238–14254.
22 C. Poriel and J. Rault-Berthelot, *J. Mater. Chem. C*, 2017, **5**, 3869–3897.
23 J. Rao, C. Zhao, Y. Wang, K. Bai, S. Wang, J. Ding and L. Wang, *ACS Omega*, 2019, **4**, 1861–1867.
24 M. Numata, T. Yasuda and C. Adachi, *Chem. Commun.*, 2015, **51**, 9443–9446.
25 L. Gan, Z. Xu, Z. Wang, B. Li, W. Li, X. Cai, K. Liu, Q. Liang and S. Su, *Adv. Funct. Mater.*, 2019, **29**, 1808088.
26 A. Khan, Y.-K. Wang, C.-C. Huang, S. Kumar, M.-K. Fung, Z.-Q. Jiang and L.-S. Liao, *Org. Electron.*, 2020, **77**, 105520.
27 F. Lucas, O. A. Ibraikulov, C. Quinton, L. Sicard, T. Heiser, D. Tondelier, B. Geffroy, N. Leclerc, J. Rault-Berthelot and C. Poriel, *Adv. Opt. Mater.*, 2020, **8**, 1901225.
28 Q. Wang and D. Ma, *Chem. Soc. Rev.*, 2010, **39**, 2387.
29 T. J. Penfold, *J. Phys. Chem. C*, 2015, **119**, 13535–13544.
30 H. Sun, C. Zhong and J.-L. Brédas, *J. Chem. Theory Comput.*, 2015, **11**, 3851–3858.
31 M. Moral, L. Muccioli, W.-J. Son, Y. Olivier and J. C. Sancho-García, *J. Chem. Theory Comput.*, 2015, **11**, 168–177.
32 A. Dreuw and M. Head-Gordon, *Chem. Rev.*, 2005, **105**, 4009–4037.
33 T. Etienne, X. Assfeld and A. Monari, *J. Chem. Theory Comput.*, 2014, **10**, 3896–3905.
34 T. Etienne, X. Assfeld and A. Monari, *J. Chem. Theory Comput.*, 2014, **10**, 3906–3914.
35 M. A. El-Sayed, *J. Chem. Phys.*, 1963, **38**, 2834.
36 T. Hosokai, H. Matsuzaki, H. Nakanotani, K. Tokumaru, T. Tsutsui, A. Furube, K. Nasu, H. Nomura, M. Yahiro and C. Adachi, *Sci. Adv.*, 2017, **3**, e1603282.
37 M. Y. Wong, S. Krotkus, G. Copley, W. Li, C. Murawski, D. Hall, G. J. Hedley, M. Jaricot, D. B. Cordes, A. M. Z. Slawin, Y. Olivier, D. Beljonne, L. Muccioli, M. Moral, J.-C. Sancho-Garcia, M. C. Gather, I. D. W. Samuel and E. Zysman-Colman, *ACS Appl. Mater. Interfaces*, 2018, **10**, 33360–33372.
38 D. Li, W. Hu, J. Wang, Q. Zhang, X.-M. Cao, X. Ma and H. Tian, *Chem. Sci.*, 2018, **9**, 5709–5715.
39 C. Adachi, *Jpn. J. Appl. Phys.*, 2014, **53**, 060101.